LPTV loop-shaping with application to non-equidistantly sampled precision mechatronics

LPTV Loop-Shaping with Application to Non-Equidistantly Sampled Precision Mechatronics

Jurgen van Zundert
Eindhoven University of Technology, The Netherlands
j.c.d.v.zundert@tue.nl

Tom Oomen
Eindhoven University of Technology, The Netherlands
t.a.e.oomen@tue.nl

***Abstract*—Flexible sampling strategies, such as non-equidistant sampling, potentially enhance the performance/cost trade-off present in traditional fixed sampling schemes. The aim of this paper is to develop a systematic feedback control design approach for systems with flexible sampling which are inherently time-varying. A framework for stability and performance analysis based on frequency response function measurements is presented. The framework enables loop-shaping feedback control design for non-equidistantly sampled systems based on LTI insights. Application of the framework in a case study demonstrates the use for feedback control design and the potential of non-equidistant sampling.**

***Index Terms*—linear periodically time-varying, frequency response functions, feedback control, loop-shaping**

I. Introduction

Control applications are typically implemented digitally with equidistant sampling to obtain lower cost and higher design freedom [1]. For linear time-invariant (LTI) systems, the equidistant sampling allows the use of well-known frequency domain control design approaches through, for example, Bode plots and Nyquist diagrams [2]. However, fixed equidistant sampling is limited to a performance/cost trade-off. For example, an increase in sampling rate to increase performance also increases the hardware cost of, e.g., sensors and actuators.

The performance/cost trade-off can be enhanced by exploiting the flexibility in sampling provided by present-day embedded software. Examples of this flexiblity are task scheduling policies leading to non-equidistant sampling of the individual tasks. Flexible sampling schemes, such as multirate control [3], [4], [5] and non-equidistant sampling [6], allow to exploit the full potential of digital control.

Traditional frequency domain control design techniques [2] assume LTI dynamics and hence cannot deal with time-varying dynamics introduced by flexible sampling. Flexible sampling, such as non-equidistant sampling, of LTI systems leads to linear periodically time-varying (LPTV) systems [6]. Model-based control designs for LPTV systems include pole placement [7], LQR/LQG, $\mathcal{H}_2/\mathcal{H}_\infty$ approaches [8], and internal model principle [9]. Also designs based on time-invariant reformulations such as Floquet-Lyapunov transformations [10, section 1.2] and lifting approaches [10, section 1.6] are often model based. However, as is argued in [11], despite the abdundant control theory, model-based designs are challenging since obtaining a parametric LPTV model is difficult, and typical LTI interpretations are not valid, complicating the actual design [12], [13].

Although control theory for LPTV systems has been significantly developed, at present there is no systematic control design approach based on frequency response function (FRF) measurements. The aim of this paper is to develop a control framework for non-equidistantly sampled systems which enables loop-shaping control design [2, section 2.6], [14], [15, section 6] based on FRF measurements only. The framework explicitly incorporates time-varying aspects and addresses key objectives such as stability and performance.

The main contribution of this paper is a framework that facilitates LPTV loop-shaping feedback control design based on FRF measurements. This paper has the following contributions: (I) stability test: an FRF measurements based Nyquist test for LPTV systems; (II) performance quantification: LPTV generalizations of FRFs; and (III) demonstration of the potential of non-equidistant sampling through application of the framework in a case study. The presented framework forms the basis for loop-shaping feedback control design for systems with flexible sampling.

The outline of this paper is as follows. In section II, the potential of non-equidistant sampling is demonstrated and the control objectives are presented. The Nyquist stability test for the non-equidistantly sampled system (contribution (I)) is presented in section III. The performance quantification based on FRFs (contribution (II)) is presented in section IV. Application of the framework is demonstrated via a case study (contribution (III)) in section V. Conclusions are provided in section VI.

II. Non-equidistant sampling in motion control

In this section, the potential of non-equidistant sampling in motion control applications is explored and the control objectives are defined.

A. Example of non-equidistant sampling

Multiple applications are often embedded on a single platform to reduce cost. The platform resources are allocated to the different applications using a scheduling policy. The required predictability of the scheduling is offered by platforms such as CompSOC [16].

Scheduling of applications is often periodic and results in periodic non-equidistant sampling of the individual applications as illustrated in Fig. 1. The non-equidistant sampling

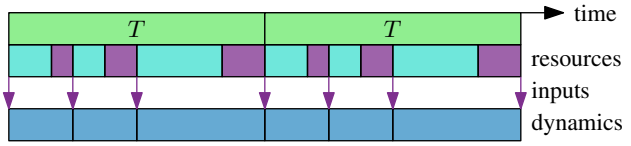

Fig. 1. Scheduling allocates resources to the different applications. For the motion task in purple this leads to non-equidistantly sampled dynamics. The scheduling is periodic with period T.

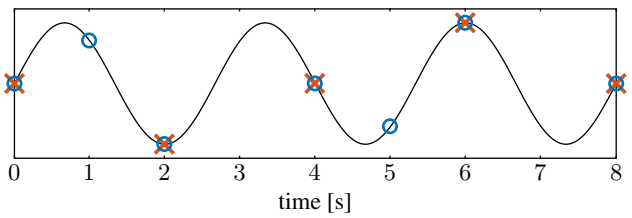

Fig. 2. Example demonstrating the potential of non-equidistant sampling. The sampling intervals of the equidistant sampling sequence (×) are too large to control the signal (——). The non-equidistant sampling sequence (○) with period 4 s has additional control points at $1, 5, \ldots$ that can be used to improve performance as the related sampling intervals are sufficiently small.

introduces time-variance, also for time-invariant applications. In particular, periodic non-equidistant sampling of a linear time-invariant (LTI) system results in linear periodically time-varying (LPTV) behavior [6], [1].

B. Exploiting non-equidistant sampling in control design

The potential of non-equidistant sampling is illustrated via the example in Fig. 2. The discrete-time controller input is given by the samples ○ of the continuous-time sine wave —— with frequency $\frac{3}{8}$ Hz. The input sequence is sampled non-equidistantly, whereas LTI control designs require equidistant sampling. Equidistant sampling can be obtained by discarding control points. The equidistant sampling sequence with the highest sampling frequency is given by the sequence × and has Nyquist frequency $\frac{1}{4}$ Hz. Hence, by the Nyquist-Shannon sampling theorem [15, section 8.4.3], LTI control designs are inadequate since the input frequency is larger than the Nyquist frequency.

Control on the non-equidistant sampling sequence ○ can be beneficial since some of the intervals have a Nyquist frequency of $\frac{1}{2}$ Hz which is larger than the input frequency $\frac{3}{8}$ Hz. Hence, non-equidistant sampling has potential in control design.

C. Control objectives

In this paper, the focus is on feedback control of non-equidistantly sampled LTI motion applications as shown in Fig. 3, where G_d^0 denotes the LTI motion system. Non-equidistant sampling of G_d^0 is represented by upsampler $\mathcal{H}$ and downsampler $\mathcal{D}$ which convert the equidistant base rate with fixed sampling interval δ^0 into the non-equidistant rate with periodically time-varying sampling intervals $\delta_i = \gamma_i \delta^0$, $\gamma_i \in \mathbb{N}$, $i = 1, 2, \ldots, \tau$, and vice versa. An example of a scheduling sequence is given in Fig. 4 where $\tau = 3$ and $\gamma_1 = \gamma_2 = 2$, $\gamma_3 = 2$, or in short $\Gamma^{ne} = [1, 1, 2]$.

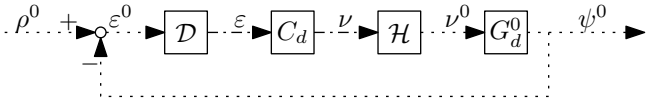

Fig. 3. Feedback control diagram with equidistant rate ^{0} (·····) and non-equidistant rate (-·-·-). The control goal is minimization of ε^0 through design of non-equidistantly sampled feedback controller C_d.

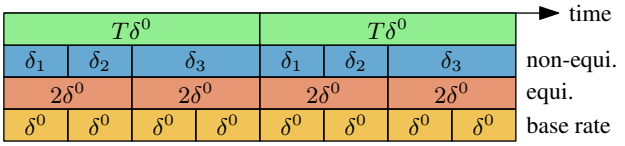

Fig. 4. The periodic scheduling ($\Gamma^{ne} = [1, 1, 2]$) results in non-equidistant sampling of the individual applications (blue). Downsampling to an equidistant sampling rate (red) is conservative in terms of performance since not all control points are exploited. The base rate (yellow) is not available for control and only used for performance evaluation.

The control objective considered in this paper is given by Problem 1.

Problem 1. *Given the control diagram in Fig. 3, an FRF measurement of G_d^0, and sampling sequence Γ^{ne}, design LPTV controller C_d through loop-shaping such that*

(A) the closed-loop system is stable; and
(B) the error ε^0 is satisfactory small.

In this paper, the stability aspect (Problem 1(A)) and the performance aspect (Problem 1(B)) are addressed in section III and section IV, respectively. In section V, stability and performance of three controllers are evaluated in a case study. A system loop-shaping control design procedure for LPTV systems is part of future research.

III. Stability: Nyquist test for LPTV systems

In this section, a stability test for the closed-loop system in Fig. 3 is presented which addresses Problem 1(A). The result is a Nyquist test for LPTV systems and constitutes contribution (I).

The Nyquist stability test is based on lifting the open-loop transfer of the system in Fig. 3. The time-lifting reformulations are presented in section III-A. The Nyquist stability test for LPTV systems is presented in section III-B.

A. Lifted reformulations

Lifting the LPTV controller C_d over its period τ is given by Lemma 1 and follows from [10, section 6.2.3].

Lemma 1. *The $\tau \in \mathbb{N}$ periodic state-space system $C_d \overset{s}{=} (A_k, B_k, C_k, D_k)$, $k = 0, 1, 2, \ldots$, with $A_{k+\tau} = A_k, B_{k+\tau} = B_k, C_{k+\tau} = C_k, D_{k+\tau} = D_k$, lifted over period τ is given by*

$$C_d^{lif}(z) \overset{s}{=} \left[\begin{array}{c|ccc|c} \Psi & \Phi_{\tau,2}B_1 & \Phi_{\tau,3}B_2 & \cdots & D_\tau \\ \hline C_1 & D_1 & 0 & \cdots & 0 \\ C_2A_1 & C_2B_1 & D_2 & \ddots & \vdots \\ \vdots & \vdots & \ddots & \ddots & 0 \\ C_\tau\Phi_{\tau,1} & C_\tau\Phi_{\tau,2}B_1 & \cdots & C_\tau B_{\tau-1} & D_\tau \end{array}\right],$$

with transition matrix

$$\Phi_{k_2,k_1} = \begin{cases} I, & k_2 = k_1, \\ A_{k_2-1}A_{k_2-2}\dots A_{k_1}, & k_2 > k_1. \end{cases}$$

and monodromy matrix $\Psi = \Phi_{\tau,0}$.

Lemma 1 is applicable to (periodic) state-space systems and hence not to the FRF measurements of G_d^0. To lift the transfer function of G_d^0 over period T, Lemma 2 is used. The result follows from [10, section 6.2.1] and can also be applied to FRF measurements by replacing z with $e^{j\omega T\delta^0}$.

Lemma 2. *The $[i,j]$-element of the LTI transfer function $G_d^0(z)$ lifted over a period $T \in \mathbb{N}$ is given by*

$$G_d^{lif}(z)[i,j] = G^{(|i-j|)}(z),$$

with $i,j = 1,2,\dots,T$, $\phi = e^{\frac{2\pi j}{T}}$, and

$$G^{(s)}(z^T) = \frac{z^s}{T}\sum_{k=0}^{T-1} G_d^0(z\phi^k)\phi^{ks}.$$

To construct the LTI reformulation of the open-loop transfer the following definition is introduced.

Definition 3. *Let*

$$\delta_T[i] := i-1, \qquad i = 1,2,\dots,T,$$

$$\delta_\tau[i] := \begin{cases} 0, & i = 1, \\ \sum_{j=1}^{i-1}\gamma_i, & i = 2,3,\dots,\tau+1, \end{cases}$$

and define $\underline{\mathcal{D}} \in \mathbb{N}^{\tau\times T}$, $\underline{\mathcal{H}} \in \mathbb{N}^{T\times\tau}$ as

$$\underline{\mathcal{D}}[i,j] := \begin{cases} 1, & \delta_\tau[i] = \delta_T[j], \\ 0, & \textit{otherwise}, \end{cases}$$

$$\underline{\mathcal{H}}[i,j] := \begin{cases} 1, & \delta_\tau[j] \le \delta_T[i] < \delta_\tau[j+1], \\ 0, & \textit{otherwise}. \end{cases}$$

B. Nyquist test

Using the time-lifted reformulations, the main result of this section can be presented, namely the Nyquist stability test for the closed-loop LPTV system in Fig. 3. The result is presented in Theorem 4 and constitutes contribution (I).

Theorem 4 (Closed-loop stability LPTV system)**.** *The closed-loop system in Fig. 3 is stable if and only if the Nyquist plot of* $\det(I + L_d^{lif})$*, with*

$$L_d^{lif}(e^{j\omega T\delta^0}) = \underline{\mathcal{D}}\, G_d^{lif}(e^{j\omega T\delta^0})\, \underline{\mathcal{H}}\, C_d^{lif}(e^{j\omega T\delta^0}), \qquad (1)$$

with G_d^{lif} in Lemma 2, C_d^{lif} in Lemma 1, and $\underline{\mathcal{D}}, \underline{\mathcal{H}}$ in Definition 3,

1) *does not pass through the origin, and*
2) *makes P_{ol} anti-clockwise encirclements of the origin,*

where P_{ol} is the number of unstable poles of L_d^{lif}.

Proof. Sketch of proof. Closed-loop stability for the system in Fig. 3 is determined by the LPTV loop transfer $L_d = \mathcal{D}G_d^0\mathcal{H}C_d$. Lifting yields the loop transfer (1) for which closed-loop stability follows from the generalized Nyquist theorem [2, Theorem 4.9]. □

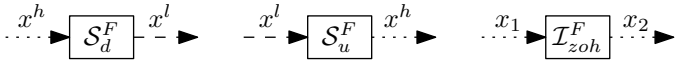

(a) Downsampler. (b) Upsampler. (c) Zero-order-hold interpolator.

Fig. 5. Multirate building blocks for conversion between equidistantly sampled signals at low rate (- - -) and at high rate (·····).

IV. Performance: frequency response functions for LPTV systems

In this section, the performance of the system in Fig. 3 is quantified which addresses Problem 1(B). The performance is quantified in terms of FRFs and constitutes contribution (II).

In section IV-A, the conversion between equidistant rates based on multirate building blocks is presented. The building blocks are used in section IV-B to describe the system in Fig. 3 through filter banks. In section IV-C, performance functions for the system in Fig. 3 are defined based on FRFs obtained from the filter banks.

A. Multirate building blocks

Conversion between equidistant rates is described by the multirate building blocks in Fig. 5, where a zero-order-hold interpolator is used. These blocks are defined in Definitions 5-7, where capital letters indicate Fourier transforms of the time-domain signals in small letters and $z \in \mathbb{C}$ is a complex indeterminate. Further properties are available in, e.g., [17, section 4.1.1].

Definition 5 (Downsampler)**.** *The downsampling operator $\mathcal{S}_d^F$ in Fig. 5(a) with downsample factor $F \in \mathbb{N}$ is defined as*

$$x^l[k] = x^h[Fk], \qquad X^l(z) = \frac{1}{F}\sum_{f=0}^{F} X^h\left(z^{\frac{1}{F}}e^{-j2\pi\frac{f}{F}}\right).$$

Definition 6 (Upsampler)**.** *The upsampling operator $\mathcal{S}_u^F$ in Fig. 5(b) with upsample factor $F \in \mathbb{N}$ is defined as*

$$x^h[k] = \begin{cases} x^l[\frac{k}{F}], & \frac{k}{F} \in \mathbb{Z}, \\ 0, & \frac{k}{F} \notin \mathbb{Z}, \end{cases} \qquad X^h(z) = X^l(z^F),$$

with $\lfloor x \rfloor = \max\{m \in \mathbb{Z} \mid m \le x\}$.

Definition 7 (Zero-order-hold interpolator)**.** *The zero-order-hold interpolator $\mathcal{I}_{zoh}^F$ in Fig. 5(c) with interpolation factor $F \in \mathbb{N}$ is defined as*

$$x_2[k] = x_1[F\lfloor\tfrac{k}{F}\rfloor], \qquad X_2 = X_1\sum_{f=0}^{F-1} z^{-f}.$$

In the next section, the multirate building blocks in Fig. 5 are used to describe the time-varying transfers in Fig. 3.

B. Filter banks

The decomposition of $\mathcal{H}C_d\mathcal{D}$ into the multirate building blocks of Fig. 5 is presented in Fig. 6, with q the forward shift operator, i.e., $qu[k] = u[k+1]$. The construction is based

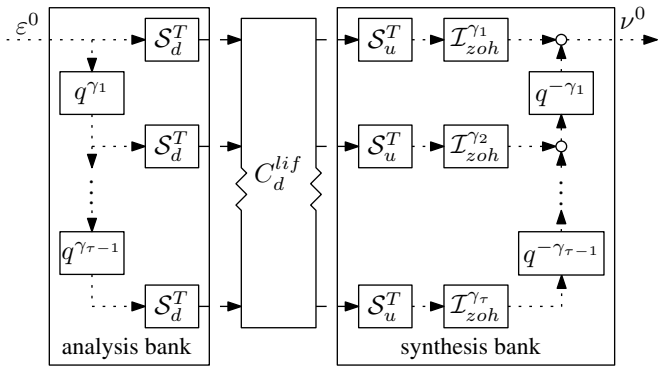

Fig. 6. Filter bank to compute the transfer $\varepsilon^0 \mapsto \nu^0$, i.e. $\mathcal{H}C_d\mathcal{D}$, in Fig. 3. The analysis bank decomposes the equidistantly sampled signal ε^0 into τ subband signals with period T. The synthesis bank constructs the equidistantly sampled signal ν^0 through upsampling with zero-order-hold interpolation. The LPTV controller C_d is lifted to the multivariable LTI system C_d^{lif} given by Lemma 1 which operates on the subband signals.

on filter banks by splitting signals into τ subband signals [17, section 4.1.2].

The filter bank of Fig. 6 describes the transfer of the non-equidistant controller, i.e., the transfer $\varepsilon^0 \mapsto \nu^0$ in Fig. 3. Other transfers follow directly through interconnection with G_d^0. For example, $\rho^0 \mapsto \varepsilon^0$ is given by $\left(I + G_d^0\mathcal{H}C_d\mathcal{D}\right)^{-1}$.

C. Performance functions LPTV system

To quantify performance, two performance functions based on FRFs are considered.

An FRF describes the relation between the Fourier transforms of the input and output. Expressing the FRF as a matrix multiplication yields the frequency response matrix (FRM). Let U be the Fourier transform of the input and Y be the Fourier transform of the output over the frequency range $[0, 2\pi)$, then for an LPTV system with period T, it holds $Y = G_{LPTV}U$ where the FRM has the structure

$$G_{LPTV} : \begin{bmatrix} \ddots & \cdots & \ddots \\ \vdots & \ddots & \vdots \\ \ddots & \cdots & \ddots \end{bmatrix} \tag{2}$$

consisting of $T \times T$ diagonal submatrices. The structure in (2) clearly shows that the frequency separation principle does not hold for LPTV systems, i.e., an input with a single frequency component may yield multiple output frequencies.

To quantify performance of the LPTV system in Fig. 3 in the frequency domain, the fundamental transfer function (FTF) $\mathcal{F}$ and the performance frequency gain (PFG) $\mathcal{P}$ are used. Both functions are commonly used for multirate and sampled-data systems, see [11], [13] and references therein. Generalizations for LPTV systems in terms of the FRM are presented in Definition 8.

Definition 8 (Performance functions $\mathcal{F}$ and $\mathcal{P}$)**.** *Let frequency response matrix G have elements $G[i, j]$ corresponding to the i^{th} output frequency and the j^{th} input frequency. For the k^{th} input frequency, the fundamental transfer function (FTF) is defined by*

$$\mathcal{F}_k = G[k, k] \tag{3}$$

and the performance frequency gain (PFG) is defined by

$$\mathcal{P}_k = \sqrt{\sum_i \left\|G[i, k]\right\|_2^2}. \tag{4}$$

The FTF corresponds to the diagonal of the FRM and hence only takes into account the fundamental frequency component. The PFG takes into account the full intersample behavior and relates the root-mean-square (rms) value of the output to that of the input. This is particularly relevant to quantify control performance as is shown by the case study in the next section.

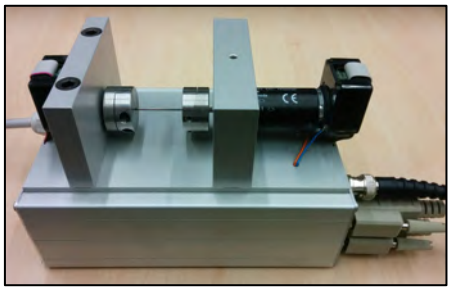

Fig. 7. Motion system consisting of two rotating masses connected by a shaft. The collocated motor and encoder form the input and output, respectively.

V. Application to non-equidistant sampling in motion control

In this section, both the stability test in section III and the performance quantification in section IV are demonstrated via a case study. The case study shows the potential of non-equidistant sampling and constitutes contribution (III).

A. Setup

The closed-loop system in Fig. 3 is considered with G_d^0 the motion system shown in Fig. 7. An FRF measurement of G_d^0 is shown in Fig. 8. The base rate is given by $\delta^0 = 0.25$ ms. The non-equidistant sampling sequence is given by $\Gamma^{ne} = [2, 2, 4]$ ($T = 8$), see also section II-B. Input ρ^0 is given by

$$\rho_k^0 = A_1 \sin(2\pi f_1 k) + A_2 \sin(2\pi f_2 k), \tag{5}$$

with $A_1 = 3.5\sqrt{2}$ rad, $f_1 = 20$ Hz, $A_2 = 1.5\sqrt{2}$ rad, $f_2 = 920$ Hz.

B. Controller design

A non-equidistant controller design is compared with an equidistant controller design. For comparison, both designs are based on downsampling the same stabilizing base rate controller. The open-loop transfer with the base rate controller is shown in Fig. 8. The controller stabilizes the system with a bandwidth (first 0 dB crossing of the open-loop) of 25 Hz.

The equidistantly sampled controller $C_{d,1}$ is obtained by sampling the base rate controller with $\Gamma^{eq} = [4, 4]$, i.e. the maximum equidistant sampling rate. The non-equidistantly

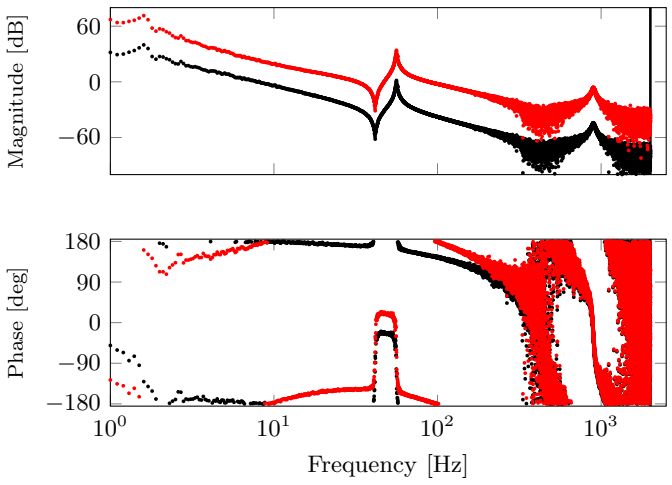

Fig. 8. FRF measurement of the system G_d^0 (•) shown in Fig. 7 and the open-loop system $G_d^0 C_d^0$ (•). The base rate controller C_d^0 stabilizes the system with a bandwidth of 25 Hz.

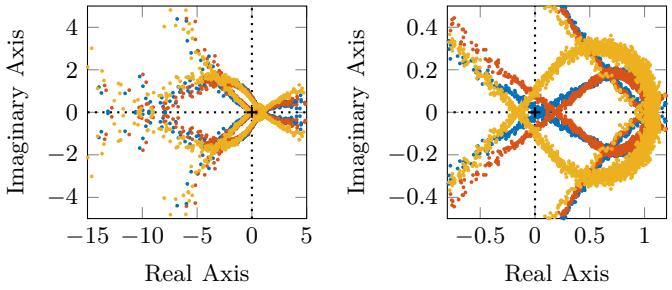

(a) View around the origin. (b) Detailed view around the origin.

Fig. 9. Nyquist diagram of $\det(I + L_{d,i}^{lif})$ for controller $C_{d,1}$ (•), controller $C_{d,2}$ (•), and controller $C_{d,3}$ (•). For $C_{d,1}$ and $C_{d,2}$ there are no net encirclements of the origin, hence the closed-loop system is stable. For $C_{d,3}$ there is one net encirclement of the origin, hence the closed-loop system is unstable. See also Theorem 4.

sampled controller $C_{d,2}$ is obtained by non-equidistant sampling of the base rate controller with Γ^{ne}, see also Fig. 6.

C. Stability

Stability of the closed-loop system in Fig. 3 is evaluated using Theorem 4. The Nyquist diagrams for both controllers are shown in Fig. 9. Using the Nyquist diagrams it is determined that both $C_{d,1}$ and $C_{d,2}$ stabilize the system.

To demonstrate that stability is nontrivial, a third controller $C_{d,3}$ is considered. The controller is based on non-equidistant sampling of a base rate controller. The base rate controller design is similar to that of C_d^0 shown in Fig. 8, but with an increased bandwidth (31 Hz). The base controller stabilizes the closed-loop system, however, $C_{d,3}$ yields an unstable closed-loop system as shown by Fig. 9. The results show that downsampling of a stabilizing controller at the base rate does not necessarily yield a stabilizing controller when implemented at a lower (non-equidistant) rate.

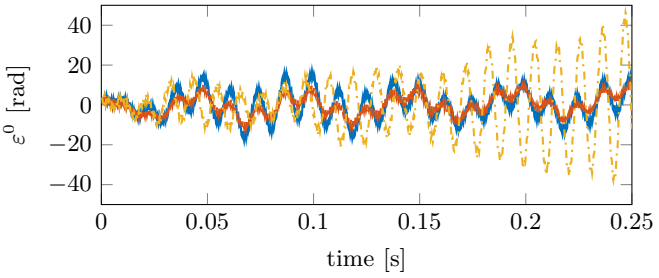

(a) Error ε^0 remains bounded for the stabilizing equidistantly sampled controller $C_{d,1}$ (——) and the stabilizing non-equidistantly sampled controller $C_{d,2}$ (– – –), whereas it grows unbounded for the non-equidistantly sampled destabilizing controller $C_{d,3}$ (–·–·–).

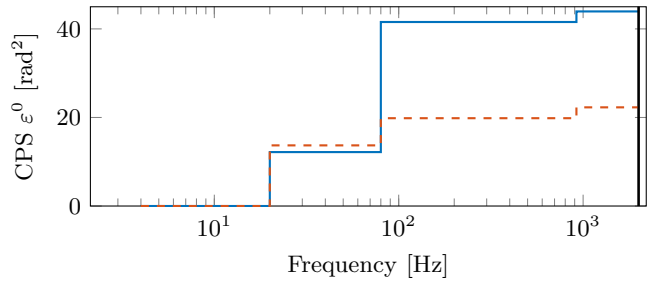

(b) Cumulative power spectrum of ε^0 for $C_{d,1}$ (——) and $C_{d,2}$ (– – –).

Fig. 10. The stability with controllers $C_{d,1}, C_{d,2}$ and instability with controller $C_{d,3}$ concluded from Fig. 9 are confirmed by analysis of ε^0.

D. Performance

The time-domain signals ε^0 for $C_{d,1}, C_{d,2}, C_{d,3}$ are shown in Fig. 10(a). The results confirm stability for $C_{d,1}, C_{d,2}$ and instability with $C_{d,3}$. The results also show that the non-equidistantly sampled controller $C_{d,2}$ outperforms the equidistantly sampled controller $C_{d,1}$. This is a direct result of the additional control points that are available and demonstrates the potential of non-equidistant sampling. Next, the performance of non-equidistantly sampled $C_{d,2}$ is further evaluated. Analysis of $C_{d,1}$ follows along similar lines.

The cumulative power spectrum (CPS) of ε^0 for $C_{d,2}$ is shown in Fig. 10(b). The CPS reveals three dominant frequencies: 20 Hz, 80 Hz, and 920 Hz. The 20 Hz and 920 Hz components correspond to frequencies f_1, f_2 in (5), respectively. The 80 Hz component is the only dominant image of f_2: $2\frac{1}{T\delta^0} - f_2 = 80$ Hz, where $\frac{1}{T\delta^0} = 500$ Hz is the periodic sampling frequency.

The magnitude of the performance functions $\mathcal{F}$ (3) and $\mathcal{P}$ (4) are shown in Fig. 11. Function $\mathcal{F}$ only shows the fundamental components, i.e., the diagonal of the FRM. In contrast, $\mathcal{P}$ shows the full behavior. The responses of both functions to input frequencies f_1, f_2 in (5) are presented in Table I. Note that $|\mathcal{F}|$ and $\mathcal{P}$ are the same for frequency f_1 since no images occur for this frequency.

The performance frequency gain $\mathcal{P}$ specifies the contribution of each input frequency to the power in the output and is therefore relevant for controller design. The contributions of the individual frequencies f_1, f_2 in ρ^0 (5) to the power in ε^0 can be determined as follows. Input frequency f_1 contributes

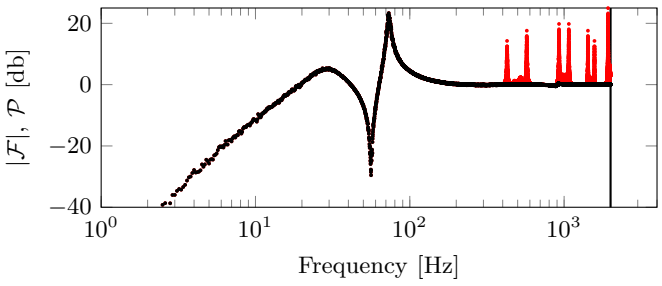

Fig. 11. Fundamental transfer function $\mathcal{F}$ (•) and performance frequency gain $\mathcal{P}$ (•) of the transfer $\rho^0 \mapsto \varepsilon^0$ for controller $C_{d,2}$. Function $\mathcal{P}$ takes into account the imaging present at high frequencies, in contrast to $\mathcal{F}$.

TABLE I
PERFORMANCE FUNCTIONS $\mathcal{F}$ AND $\mathcal{P}$ FOR $C_{d,2}$ SHOWN IN FIG. 11, EVALUATED AT FREQUENCIES f_1, f_2 IN (5). FOR f_1, $|\mathcal{F}| = \mathcal{P}$, WHEREAS FOR f_2, $|\mathcal{F}| \neq \mathcal{P}$ DUE TO IMAGING.

	$\mathcal{F}$	$\lvert\mathcal{F}\rvert$ [dB]	$\mathcal{P}$	$\mathcal{P}$ [dB]
$f_1 = 20$ Hz	$-0.343 + 1.000j$	0.484	1.057	0.484
$f_2 = 920$ Hz	$1.043 + 0.030j$	0.373	1.954	5.818

$\left(\frac{A_1}{\sqrt{2}}\mathcal{P}_{f=f_1}\right)^2 = (3.5 \cdot 1.057)^2 = 13.695$ to the power of ε^0 which corresponds to the first plateau in Fig. 10(b). Input frequency f_2 contributes $\left(\frac{A_2}{\sqrt{2}}\mathcal{P}_{f=f_2}\right)^2 = (1.5 \cdot 1.954)^2 = 8.589$ to the power of ε^0 which corresponds to the difference between the third and first plateau in Fig. 10(b). Note that frequency f_2 yields multiple contributions (where 80 Hz and 920 Hz are dominant) as a result of imaging. The total power in ε^0 is the sum of the individual contributions $\sum_{i=1}^{2}\left(\frac{A_i}{\sqrt{2}}\mathcal{P}_{f=f_i}\right)^2 = 22.285$, and corresponds to the CPS value at the Nyquist frequency of 2000 Hz in Fig. 10(b).

A similar reasoning can be followed for controller $C_{d,1}$. The analysis shows how the PFG can be used to quantify performance of (non-)equidistantly sampled systems.

E. Summary

The case study shows the application of the presented framework for both stability and performance analysis of non-equidistantly sampled systems. In particular, it shows that (I) closed-loop stability at the equidistant base rate is not preserved when downsampling the controller to a non-equidistant rate; (II) the power frequency gain is relevant to quantify performance for control design; and (III) non-equidistant sampling has a large potential in (motion) control.

VI. CONCLUSIONS

Flexible sampling, such as non-equidistant sampling, has the potential to enhance the performance/cost trade-off in traditional fixed sampling. However, at present there is no practical control design framework for systems with non-equidistant sampling. In this paper, a framework to test stability and quantify performance of non-equidistantly sampled systems is presented. The framework is based on FRFs and facilitates loop-shaping feedback controller design based on FRF measurements.

In future work, a loop-shaping control design procedure for non-equidistantly sampled systems will be presented based on the presented framework.

ACKNOWLEDGMENTS

The authors would like to acknowledge the important contributions of Niek Wolma to the presented work.

This work is part of the research programmes Robust Cyber-Physical Systems (RCPS) (No. 12694) and VIDI (No. 15698); both are (partly) financed by the Netherlands Organisation for Scientific Research (NWO).

REFERENCES

[1] T. Chen and B. A. Francis, *Optimal Sampled-Data Control Systems*. London, Great Britain: Springer, 1995.

[2] S. Skogestad and I. Postlethwaite, *Multivariable feedback control: analysis and design*. Wiley New York, 2005, vol. 2.

[3] H. Fujimoto, Y. Hori, and A. Kawamura, "Perfect Tracking Control Based on Multirate Feedforward Control with Generalized Sampling Periods," *Transactions on Industrial Electronics*, vol. 48, no. 3, pp. 636–644, 2001.

[4] J. Salt and P. Albertos, "Model-Based Multirate Controllers Design," *Transactions on Control Systems Technology*, vol. 13, no. 6, pp. 988–997, 2005.

[5] J. van Zundert, J. Verhaegh, W. Aangenent, T. Oomen, D. Antunes, and W. Heemels, "Feedforward for Multi-Rate Motion Control: Enhanced Performance and Cost-Effectiveness," in *Proceedings of the 2015 American Control Conference*, Chicago, Illinois, 2015, pp. 2831–2836.

[6] J. van Zundert, T. Oomen, D. Goswami, and W. Heemels, "On the Potential of Lifted Domain Feedforward Controllers with a Periodic Sampling Sequence," in *Proceedings of the 2016 American Control Conference*, Boston, Massachusetts, 2016, pp. 4227–4232.

[7] M. Kono, "Eigenvalue assignment in linear periodic discrete-time systems," *International Journal of Control*, vol. 32, no. 1, pp. 149–158, 1980.

[8] J. Nie, R. Conway, and R. Horowitz, "Optimal H_∞ Control for Linear Periodically Time-Varying Systems in Hard Disk Drives," *Transactions on Mechatronics*, vol. 18, no. 1, pp. 212–220, 2013.

[9] O. M. Grasselli and S. Longhi, "Robust tracking and regulation of linear periodic discrete-time systems," *International Journal of Control*, vol. 54, no. 3, pp. 613–633, 1991.

[10] S. Bittanti and P. Colaneri, *Periodic Systems - Filtering and Control*. London, Great Britain: Springer-Verlag, 2009.

[11] T. Oomen, M. van de Wal, and O. Bosgra, "Design framework for high-performance optimal sampled-data control with application to a wafer stage," *International Journal of Control*, vol. 80, no. 6, pp. 919–934, 2007.

[12] M. Cantoni and K. Glover, "Frequency-domain analysis of linear periodic operators with application to sampled-data control design," in *Proceedings of the 36th Conference on Decision and Control*, vol. 5, San Diego, California, 1997, pp. 4318–4323.

[13] O. Lindgärde and B. Lennartson, "Performance and Robust Frequency Response for Multirate Sample-Data Systems," in *Proceedings of the 1997 American Control Conference*, Albuquerque, New Mexico, 1997, pp. 3877–3881.

[14] M. Steinbuch, R. J. E. Merry, M. L. G. Boerlage, M. J. C. Ronde, and M. J. G. van de Molengraft, "Advanced Motion Control Design," in *The Control Handbook: Control Systems Applications*, 2nd ed., W. S. Levine, Ed. CRC Press, 2010, ch. 27, p. 25.

[15] G. F. Franklin, J. D. Powell, and A. Emami-Naeini, *Feedback Control of Dynamic Systems*, 7th ed. Pearson, 2015.

[16] K. Goossens, A. Azevedo, K. Chandrasekar, M. D. Gomony, S. Goossens, M. Koedam, Y. Li, D. Mirzoyan, A. Molnos, A. B. Nejad, A. Nelson, and S. Sinha, "Virtual Execution Platforms for Mixed-Time-Criticality Systems: The CompSOC Architecture and Design Flow," *ACM SIGBED Review*, vol. 10, no. 3, pp. 23–34, 2013.

[17] P. P. Vaidyanathan, *Multirate Systems and Filter Banks*. Upper Saddle River, New Jersey: Prentice-Hall, Inc., 1993.